RSC Advances

COMMUNICATION

View Article Online
View Journal | View Issue



Cite this: *RSC Adv.*, 2015, **5**, 8422

Received 2nd December 2014
Accepted 15th December 2014

DOI: 10.1039/c4ra15607b

www.rsc.org/advances



# Rigid three-dimensional $Ni_3S_4$ nanosheet frames: controlled synthesis and their enhanced electrochemical performance†

Lina Wang,[a] Jiajia Liu,*[a] Li Li Zhang,[b] Baosong Dai,[a] Meng Xu,[a] Muwei Ji,[a] X. S. Zhao,[c] Chuanbao Cao,[a] Jiatao Zhang*[a] and Hesun Zhu[a]

Rigid three-dimensional (3D) $Ni_3S_4$ nanosheet frames assembled from ultrathin nanosheets are synthesized *via* a facile solvothermal method. Compared to flat $Ni_3S_4$ sheets, 3D $Ni_3S_4$ nanosheet frames have both a high free volume and high compressive strength. They can deliver a very high specific capacitance of 1213 F $g^{-1}$ with good rate performance. In addition, these 3D $Ni_3S_4$ nanosheet frames are stabilized by plastically deformed ridges. The stabilized nanosheet frames did not unfold or collapse during electrochemical tests, and thus showed enhanced cycling ability.

Nowadays, metal chalcogenide materials have been attracting significant attention in the energy field, due to their high theoretical capacitance and low cost.[1] Key to their further development in these areas has been their improved surface area and the rigidity in their structure.[2] To date, two-dimensional (2D) metal chalcogenide nanocrystals have provided a much higher specific surface area compared with their bulk counterparts, which is beneficial to energy devices, because the reaction/interaction between the devices and the interacting media can be significantly enhanced.[3] However, during the electrode fabrication process, the nanosheet-like materials, such as graphene, tend to aggregate or restack due to strong inter-sheet van der Waals attraction.[4] Consequently, many of the unique properties that individual sheets possess, such as high specific surface area and peculiar electron transport behaviours, are significantly compromised or are even unavailable during assembly. An efficient strategy to prevent nanosheet aggregation and thus to improve the energy storage performance of sheet-like materials is to synthesize three-dimensional (3D) architectures assembled with nanosheets, such as by fabricating sandwich-type structures by introducing "spacer" (*e.g.* carbon nanotubes, nanoparticles)[5] and forming 3D macroporous structures.[6] For instance, Luo *et al.*[7] crumpled graphene sheets into paper ball-like, fractal-dimensional particles to make them aggregation-resistant in both solvents and the solid state, even after mechanical compression. Therefore, the preparation of large-area, aligned nanoporous nanostructured films in a highly crystalline state with well-oriented frameworks, excellent accessibility, and controlled porosity is an effective way to prepare metal chalcogenide-based electrode materials.

As an important class of transition metal chalcogenides, nickel sulphides with a controlled morphology is of great interest, due to their potential applications in hydrogenation catalysts and as electrode materials.[8] The electrochemical performances of the electrode materials are strongly dependent on their sizes, morphologies and structures, and up to now, some progress has been made on nickel sulphide-based electrodes. For example, Hou *et al.*[9] first investigated the potential application of NiS nanoparticles as a supercapacitor electrode and proposed an electrochemical reaction mechanism. Subsequently, Zhu *et al.*[10] reported the synthesis of hierarchical NiS hollow spheres by a template-engaged conversion method. Due to the unique structural features and high surface area, these NiS hollow spheres showed a high specific capacitance of 583–927 F $g^{-1}$ at various currents densities of 4.08–10.2 A $g^{-1}$. Later, Yang *et al.*[11] synthesized a hierarchical flower-like β-NiS electrode with a high specific discharge capacitance of 857.76 F $g^{-1}$. Recently, Pang *et al.*[12] reported the synthesis of uniform $NiS_2$ nanocubes, and these $NiS_2$ nanocube electrodes showed a large specific capacitance (695 F $g^{-1}$ at 1.25 A $g^{-1}$) and excellent cycling performance. However, $Ni_3S_4$ has attracted much less attention compared to other binary nickel sulfides, such as NiS, $Ni_3S_2$, and $NiS_2$, due to the synthetic challenges in obtaining the single phase $Ni_3S_4$.[13] $Ni_3S_4$ has a cubic spinel structure and is found in nature as the mineral polydymite.[14] Much effort has

[a]*School of Materials Science & Engineering, Beijing Institute of Technology, Beijing 100081, P. R. China. E-mail: liujiajia@bit.edu.cn; zhangjt@bit.edu.cn; Fax: +86-10-68918065; Tel: +86-10-68918065*

[b]*Institute of Chemical and Engineering Sciences, A*STAR, 1 Pesek Road, Jurong Island 627833, Singapore*

[c]*School of Chemical Engineering, The University of Queensland, St Lucia, Brisbane, QLD 4072, Australia*

† Electronic supplementary information (ESI) available. See DOI: 10.1039/c4ra15607b

been devoted to obtain single-phase $Ni_3S_4$ efficiently in laboratories. Through a selective control of the reaction conditions, such as the Ni precursor or capping agents, it is possible to obtain single phase $Ni_3S_4$ triangular nanoprisms and nanopyramids.[15] Despite the success in the synthesis of various morphologies, the preparation of uniform 3D $Ni_3S_4$ nanosheet structure in a highly crystalline state still remains a significant challenge.

Herein, we present a facile, one-pot solvothermal route to prepare rigid 3D single-crystalline $Ni_3S_4$ nanosheet frames. To the best of our knowledge, the controlled synthesis of rigid 3D $Ni_3S_4$ nanosheet frames has not been reported. As a demonstration, the obtained 3D $Ni_3S_4$ nanosheet frames were used as the electrode of a supercapacitor and demonstrated excellent electrochemical performance, even outperforming most of the nickel sulfide-based electrodes from previous reports. We anticipate that the unique 3D $Ni_3S_4$ structure originating from the ultrathin $Ni_3S_4$ nanosheet is worth further exploring for its intrinsic properties in the fields of catalysis, cathode materials in lithium batteries, and so on.

In a typical reaction, a mixture of nickel stearate, oleic acid, *n*-dodecanethiol and toluene was added in to a Teflon-lined stainless autoclave. After continuous stirring for 5 min, the reaction solution was heated up to 200 °C for 2.5 h. Once the reaction was finished and cooled down to room temperature, the black products precipitated at the bottom of the autoclave were purified with excess ethanol by centrifugation, and were then easily dispersed in ethanol for further characterization.

The typical rigid 3D $Ni_3S_4$ nanosheet frames are displayed in Fig. 1. The size and morphology of the as-prepared frames were characterized by transmission electron microscopy (TEM). A panoramic view of the 3D frames (see Fig. 1A) reveals that the sample consists entirely of a 3D frame structure, with many ridges and vertices. The scanning transmission electron microscopy (STEM) (see Fig. 1B) and the high resolution transmission electron microscope (HRTEM) images (see Fig. 1C and D) show that the average size of the 3D nickel sulfide frames is ~160 nm, and that they are assembled from very thin $Ni_3S_4$ sheets. The crystallographic phase of the nickel sulfide nanostructures was investigated by X-ray diffraction (XRD) (see Fig. 1F). The position of the diffraction peaks is in good accordance with the standard pattern of the cubic $Ni_3S_4$ (ICDD-JCPDS card no. 76-1813), indicating that the sample consists of pure single crystalline $Ni_3S_4$. It is worth noting that the 3D structures result in an apparent enhancement in peak (311) and a decrease in peak (111) of the $Ni_3S_4$ diffraction patterns. The single-crystalline feature of the $Ni_3S_4$ frames was further verified by HRTEM (see Fig. 1E). The lattice spacing of ~0.54 and ~0.33 nm matches well with the interplanar spacing of the (111) and (220) planes of the cubic $Ni_3S_4$, respectively. In addition, the selected area electron diffraction pattern from the edges shows strong $Ni_3S_4$ (111) and (220) diffraction spots, corresponding to the d-spacing of 0.54 nm and 0.33 nm, respectively. These results clearly demonstrate that the 3D $Ni_3S_4$ frame is composed of pure and single crystalline cubic $Ni_3S_4$ ultrathin nanosheets. It is notable that the obtained 3D $Ni_3S_4$ frames are very open, but are also rigid. No morphology change was observed after

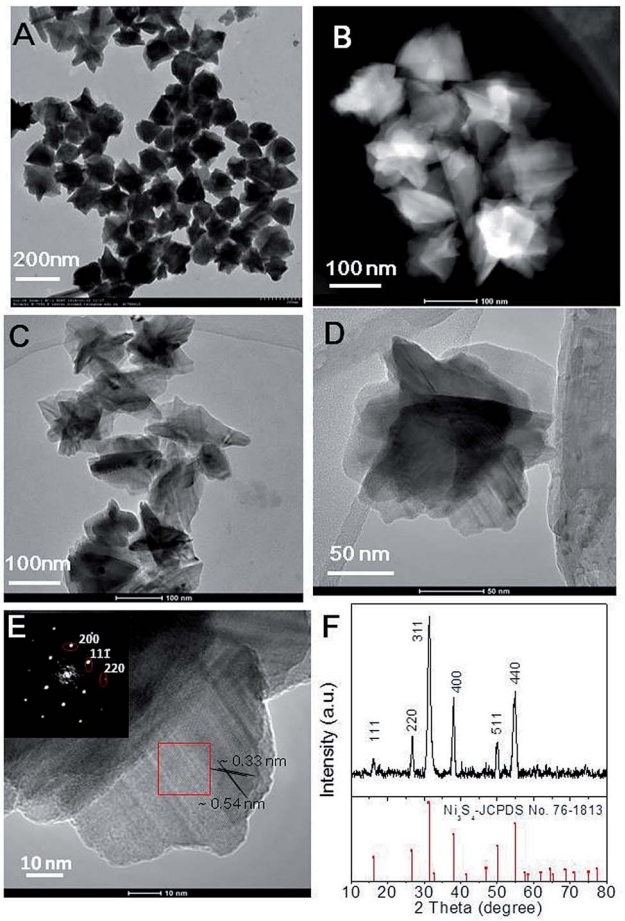


Fig. 1 TEM image (A), STEM image (B), HRTEM images (C–E), inset FFT and XRD pattern (F) of the 3D $Ni_3S_4$ nanosheet frames.

30 min ultrasonication, further implying their good structural integrity and stability (see Fig. S1†).

When the ratio of *n*-dodecanethiol/oleic acid (DDT/OA) in the reaction system was increased, while keeping all the other parameters unchanged, relative flat nickel sulfide sheets were obtained. Fig. 2A shows a typical TEM image of the as-prepared nickel sulfide products, most of which exhibit a sheet-like morphology. The XRD pattern of the nickel sulfide sheets is similar to that of the $Ni_3S_4$ 3D frames (see Fig. 2B), except there is no decrease in the intensity of the (111) peak of the $Ni_3S_4$ diffraction patterns. The HRTEM image (see Fig. 2C) reveals that the $Ni_3S_4$ sheets have near rectangular shape, with an average lateral size of ~130 nm. The thickness of the sheet was determined with an atomic force microscope (AFM, see Fig. 2D). Prominently, the thickness was measured to be only 1.0 nm.

Our experimental results imply that the ratio of DDT/OA plays an important role in tuning the structure of $Ni_3S_4$, since the only varying parameter in preparing the 3D $Ni_3S_4$ frames and flat $Ni_3S_4$ sheets is the ratio of DDT/OA; *n*-dodecanethiol is also the source of sulfur for the formation of $Ni_3S_4$. Controlled experiments were carried out to investigate the evolution of the $Ni_3S_4$ sheets and 3D frames by varying the ratio of DDT/OA and the reaction time. The evolution of the morphology was

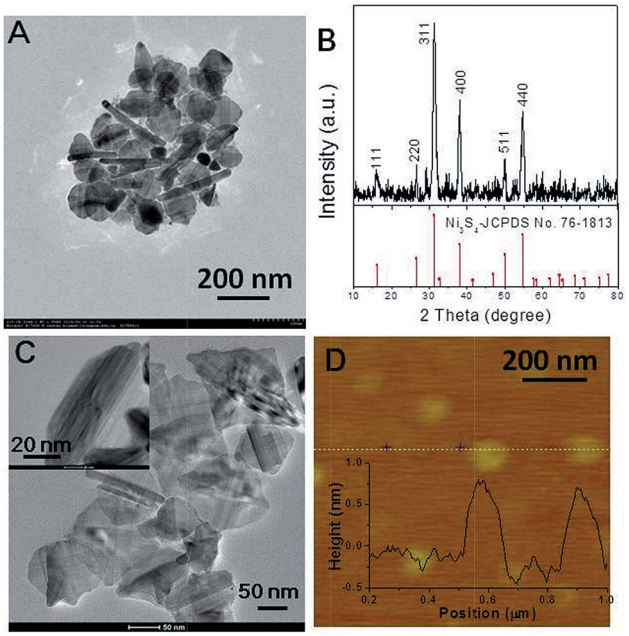


Fig. 2 TEM image (A), XRD pattern (B), HRTEM images (C), AFM image with height information data (D) of the flat $Ni_3S_4$ sheets.

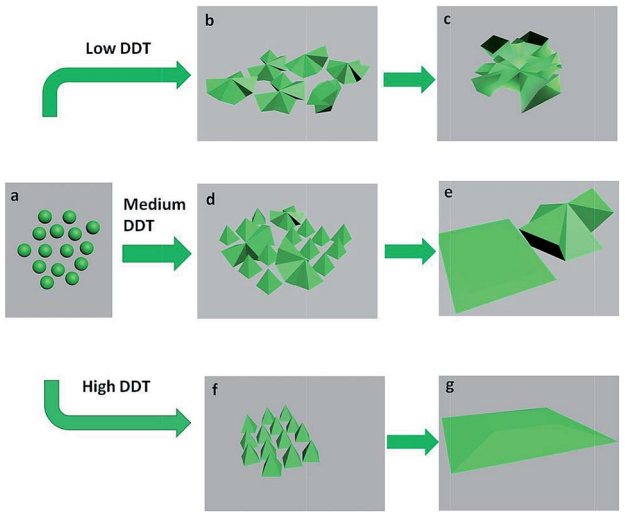


Scheme 1 Schematic illustration of the proposed mechanism for the formation of the 3D $Ni_3S_4$ nanosheet frames and $Ni_3S_4$ sheets.

examined by TEM, as shown in Fig. S2–S4.† At a medium ratio of DDT/OA (*e.g.* 0.6 ml/6 ml or 0.8 ml/6 ml), the final product is composed of both sheets and 3D frames (see Fig. S2†). The sample prepared at a low ratio (*e.g.* 0.5 ml/6 ml) and collected in the early stages (0.5 h, 1.0 h, 1.5 h) exhibit an immature 3D assembly structure, and the size and the sharpness of the 3D structure increases with the extension of time (see Fig. S3†). The sample prepared at a high ratio (*e.g.* 1 ml/6 ml) and collected in the early stages (0.5 h, 1.0 h, 1.5 h) (see Fig. S4†) exhibits a sheet structure, and the size of sheet increases with the extension of time (see Fig. S4†). From the HRTEM image of a single relative small $Ni_3S_4$ 3D frame (see Fig. S5†), the clear lattice fringes at the extended end are visible and the interplanar distance is measured as ~0.54 nm and ~0.29 nm, corresponding to the (111) and (311) planes. This indicates that the growth direction is along the [311] direction. The growth rate of the {111} crystallographic facet was lower than that of the {311} facet, which is consistent with the intensity ratio for the (111) *vs.* the (311) peak (see Fig. 1F), in a qualitative manner. According to these observations and the previous literature,[16] we propose that both the $Ni_3S_4$ sheets and the 3D frames could be obtained from the coalescence of the $Ni_3S_4$ nucleus (see Scheme 1a) in an oriented way. In the initial stages, $Ni_3S_4$ nanopyramids (see Scheme 1f) are formed in the reaction system. When the ratio of DDT/OA is low, the $Ni_3S_4$ nanopyramids tend to aggregate to minimize the total surface energy, and thus small $Ni_3S_4$ nano-aggregates are formed through a self-assembly process (see Scheme 1b). As the reaction continues, the growth rate of the {111} facets was lower than that of the {311} facets, which results in growth along the [311] direction, and finally leads to the formation of $Ni_3S_4$ 3D frames assembled from the thin $Ni_3S_4$ nanosheets (see Scheme 1c). On the other hand, the higher DDT/OA ratio results in well-dispersed $Ni_3S_4$ nanopyramids initially (see Scheme 1f). As the reaction goes on, the reaction system tends to minimize the total energy by forming relatively flat $Ni_3S_4$ sheets through the coordination of *n*-dodecanethiol and oleic acid (see Scheme 1g). When the DDT/OA ratio is at a medium level, both 3D frames and relatively flat sheets are formed in the reaction system (see Scheme 1e).

A good electrode material for a pseudocapacitor should have a large specific surface area and a suitable pore-size distribution which allows efficient contact between the electroactive sites and the electrolyte ions for fast faradic energy storage.[17] Since the $Ni_3S_4$ 3D frames are a highly open structure, they should have a higher specific surface area than the stacked flat $Ni_3S_4$ sheets. Indeed, nitrogen adsorption/desorption analysis reveals that $Ni_3S_4$ 3D frames have a higher BET surface area (122.6 $m^2\ g^{-1}$) than the flat $Ni_3S_4$ sheets (66.7 $m^2\ g^{-1}$). The value is also higher than some other nickel sulfide nanomaterials reported in the literature, such as NiS hierarchical hollow microspheres (34.3 $m^2\ g^{-1}$)[18] and hierarchical flower-like β-NiS nanostructures (24.0615 $m^2\ g^{-1}$).[19] The nitrogen adsorption/desorption isotherm of the $Ni_3S_4$ 3D frames (see Fig. 3A) displays a type-IV isotherm with a type-H3 hysteresis loop in the

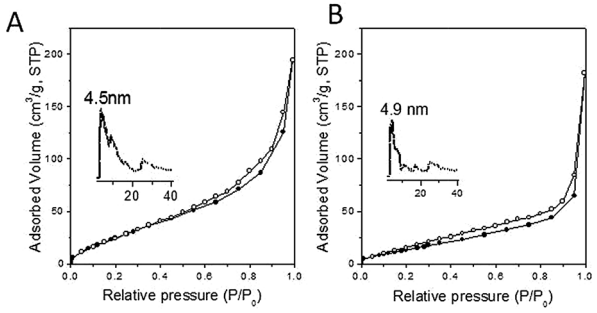


Fig. 3 $N_2$-sorption isotherms and pore size distribution (inset) of the $Ni_3S_4$ 3D frames (A) and flat $Ni_3S_4$ sheets (B).

relative pressure range of 0.6–1.0 $p/p_0$, indicating the presence of a mesoporous structure. SEM images of the working electrode are shown in Fig. S6.† As expected, the flat $Ni_3S_4$ nanosheets are packed like a stack of papers, with a smooth featureless surface. For the 3D $Ni_3S_4$ nanosheet frames, the surface has essentially indistinguishable microstructures. It should be noted that there is free space inside each individual 3D nanosheet frame, as well as between them.

The electrochemical properties of the $Ni_3S_4$ 3D frames and flat $Ni_3S_4$ sheets were studied in 3 M KOH aqueous solution using a three-electrode system. Their typical cyclic voltammetry (CV) curves at a scan rate of 5 mV $s^{-1}$ are shown in Fig. 4A. There can be seen a pair of redox peaks in the potential range of −0.15–0.55 V (*vs.* SCE). For nickel sulfide-based electrodes, it is widely accepted that the storage mechanism is mainly based on the surface redox reaction between $Ni^{2+}$ and $Ni^{3+}$.[9,11,19] It is observed from the CV curves that the $Ni_3S_4$ 3D frame electrode has a higher electrochemical activity. The rate capability of the $Ni_3S_4$ 3D frame-based electrode is illustrated in Fig. S7A† at different scan rates. With the increasing scan rate, the shape of the curves is maintained, suggesting a relatively good rate performance. Moreover, the peak current increases and the oxidation peak shifts to a more positive position, while the reduction peak shifts to a more negative position. This is due to the increased internal resistance within the pseudoactive material with the increase in scan rate.

Consistent with the CV results, the plateaus in the charge–discharge curves (see Fig. 4B) indicate the existence of faradic processes. The ability for a high-rate discharge is crucial for a pseudocapacitor. Galvanostatic charge–discharge curves of the $Ni_3S_4$ 3D frame-based electrode at different current densities are shown in Fig. S7B,† and the corresponding rate dependent specific capacitances as a function of current density for $Ni_3S_4$ 3D frame and $Ni_3S_4$ sheet-based electrodes are shown in Fig. 4C. The $Ni_3S_4$ 3D frame electrode displays a high capacitance of 1213 F $g^{-1}$ and 587 F $g^{-1}$ at the current densities of 2 A $g^{-1}$ and 12 A $g^{-1}$, respectively; while, the capacitance of the $Ni_3S_4$ sheet electrode is only 789 F $g^{-1}$ and 324 F $g^{-1}$, respectively. The specific capacitance of our $Ni_3S_4$ 3D frame electrode is significantly larger than some nickel sulfide-based electrodes from previous studies, such as NiS hollow spheres (927 F $g^{-1}$ at 4.08 A $g^{-1}$),[10] flower-like β-NiS (857.76 F $g^{-1}$ at 2 A $g^{-1}$),[11] and $NiS_2$ nanocubes (695 F $g^{-1}$ at 1.25 A $g^{-1}$).[12] The good pseudocapacitive performance of the $Ni_3S_4$ 3D frame electrode could be attributed to its unique structural features. Specifically, the high surface area and open structure composed of ultrathin nanosheets can provide not only a high interfacial area between the electrode material and the electrolyte, but can also allow fast ionic diffusion.[10] Fig. 4D shows the cycling performance of the as-prepared electrodes at a current density of 2 A $g^{-1}$ in a voltage window of 0–0.4 V. The initial capacitance of the $Ni_3S_4$ 3D frame electrode is 1213 F $g^{-1}$, and around 60% of the initial capacitance was retained after 2000 cycles, indicating a relatively high cycling stability; while, the capacitance of the $Ni_3S_4$ sheet electrode dropped to 449 F $g^{-1}$ after 2000 cycles, and around 56% of the initial capacitance was retained. The cycling performance of our $Ni_3S_4$ 3D frame electrode is better than some nickel sulfide-based electrodes from literature, such as NiS hollow spheres (52% retention after 2000 cycles)[10] and flower-like β-NiS (44% retention after 1000 cycles).[11] This improved capacitance retention may be attributed to the enhanced structural integrity of these rigid 3D $Ni_3S_4$ nanosheet frames, which are stabilized by plastically deformed ridges.

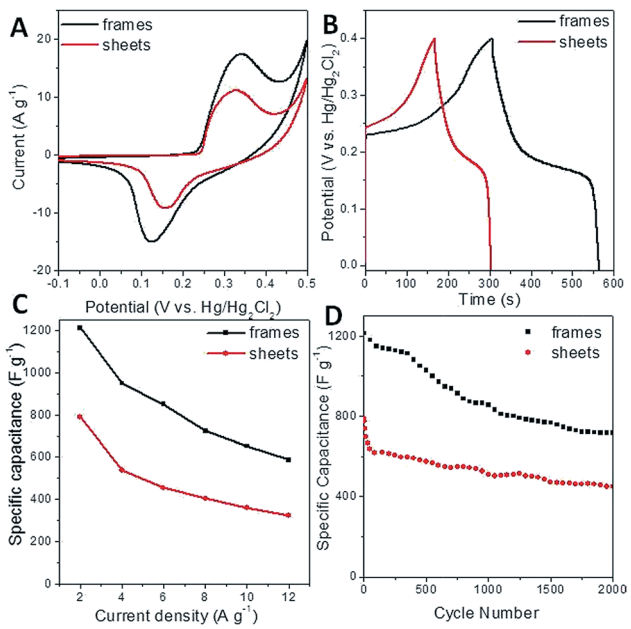


Fig. 4 The cyclic voltammogram curves at a scan rate of 5 mV $s^{-1}$ (A), the galvanostatic charge–discharge curves at a current density of 2 A $g^{-1}$ (B), the specific capacitance as a function of current density (C), and the dependence of the discharge specific capacitance on the charge–discharge cycle numbers at a current density of 2.0 A $g^{-1}$ (D) of the $Ni_3S_4$ 3D frame electrode and the flat $Ni_3S_4$ sheet electrode, respectively.

## Conclusions

In summary, a facile one-pot solvothermal method has been developed to prepare rigid 3D $Ni_3S_4$ nanosheet frames. The as-prepared 3D $Ni_3S_4$ nanosheet frames are shown to be very uniform in size, with an open and rigid structure. The DDT/OA ratio is shown to play an important role in altering the morphology of the $Ni_3S_4$ nanostructure; for instance, relatively flat $Ni_3S_4$ sheets were obtained with a high DDT/OA ratio. In virtue of its unique structure, the 3D $Ni_3S_4$ nanosheet frame electrode exhibits a high specific capacitance of 1213 F $g^{-1}$ at the current density of 2 A $g^{-1}$. Moreover, over 60% of the initial capacitances can be retained after 2000 cycles. This suggests its promising application as an electrode material for high-performance pseudocapacitors. Furthermore, we anticipate that this simple solvothermal method can be extended to the synthesis of other 3D metal sulfide nanostructures.

## Acknowledgements

We acknowledge funding by the NNSF (91123001, 21322105, and 51372025), the Research Fund for the Doctoral Program of Higher Education of China (2011101120016), Beijing Excellent

Talent Project (2012D009011000007) and Program for New Century Excellent Talents in University (NCET-11-0793).

## Notes and references

1 J. H. Han, S. Lee and J. Cheon, *Chem. Soc. Rev.*, 2013, **42**, 2581; M. Gao, Y. Xu, J. Jiang and S. Yu, *Chem. Soc. Rev.*, 2013, **42**, 2986.

2 J. L. Mohanan, I. U. Arachchige and S. L. Brock, *Science*, 2005, **307**, 397; J. B. Rivest, R. Buonsanti, T. E. Pick, L. Zhu, E. Lim, C. Clavero, E. Schaible, B. A. Helms and D. J. Milliron, *J. Am. Chem. Soc.*, 2013, **135**, 7446.

3 J. Feng, X. Sun, C. Wu, L. Peng, C. Lin, S. Hu, J. Yang and Y. Xie, *J. Am. Chem. Soc.*, 2011, **133**, 17832; Y. Du, Z. Yin, J. Zhu, X. Huang, X. WU, Z. Zeng, Q. Yan and H. Zhang, *Nat. Commun.*, 2012, **3**, 1; Z. Zeng, T. Sun, J. Zhu, X. Huang, Z. Yin, G. Lu, Z. Fan, Q. Yan, H. H. Hng and H. Zhang, *Angew. Chem., Int. Ed.*, 2012, **51**, 9052; X. Zhang, J. Zhang, J. Zhao, B. Pan, M. Kong, J. Chen and Y. Xie, *J. Am. Chem. Soc.*, 2012, **134**, 11908; J. S. Son, X. Wen, J. Joo, J. Chae, S. Bake, K. Park, J. H. Kim, K. An, J. H. Yu, S. G. Kwon, S. Choi, Z. Wang, Y. Kim, Y. Kuk, R. Hoffmann and T. Hyeon, *Angew. Chem., Int. Ed.*, 2009, **48**, 6861.

4 J. Luo, H. D. Jang, T. Sun, L. Xiao, Z. He, A. P. Katsoulidis, M. G. Kanatzides, J. M. Gibson and J. Huang, *ACS Nano*, 2011, **5**, 8943.

5 Y. Li, Z. Li and P. K. Shen, *Adv. Mater.*, 2013, **25**, 2474; L. Zhang, S. Zhao, X. N. Tian and X. S. Zhao, *Langmuir*, 2010, **26**, 17624; L. Zhang, Z. Xiong and X. S. Zhao, *J. Power Sources*, 2013, **222**, 326.

6 S. Zhang, Y. Li and N. Pan, *J. Power Sources*, 2012, **206**, 476; J. Chen, K. Sheng, P. Luo, C. Li and G. Shi, *Adv. Mater.*, 2012, **24**, 4569; S. Yin, Z. Niu and X. Chen, *Small*, 2012, **8**, 2458.

7 J. Luo, J. Kim and J. Huang, *Acc. Chem. Res.*, 2013, **46**, 2225; J. Luo, H. Jang and J. Huang, *ACS Nano*, 2013, **7**, 1464.

8 W. Wei, L. Mi, Y. Gao, Z. Zheng, W. Chen and X. Guan, *Chem. Mater.*, 2000, **35**, 3523, DOI: 10.1021/cm5006482; J. Yang, C. Bao, K. Zhu, T. Yu, F. Li, J. Liu, Z. Li and Z. Zou, *Chem. Commun.*, 2014, **50**, 4832; C. Wei, Q. Lu, J. Sun and F. Gao, *Nanoscale*, 2013, **5**, 12224.

9 L. Hou, C. Yuan, D. Li, L. Yang, L. Shen and F. Zhang, *Electrochim. Acta*, 2011, **56**, 7254.

10 T. Zhu, Z. Wang, S. Ding, J. S. Chen and X. W. Lou, *RSC Adv.*, 2011, **1**, 397.

11 J. Yang, X. Duan, Q. Qin and W. Zheng, *J. Mater. Chem.*, 2013, **1**, 7880.

12 H. Pang, C. Wei, X. Li, G. Li, Y. Ma, S. Li, J. Chen and J. Zhang, *Sci. Rep.*, 2013, **4**, 3577.

13 N. Mahmood, C. Zhang and Y. Hou, *Small*, 2013, **9**, 1321; X. Jiang, Y. Xie, J. Lu, L. Zhu, W. He and Y. Qian, *Adv. Mater.*, 2001, **13**, 1278; Y. Hu, J. Chen, W. Chen, X. Lin and X. Li, *Adv. Mater.*, 2003, **15**, 726.

14 G. Kullerud and R. A. Yund, *J. Petrol.*, 1962, **3**, 126.

15 A. L. Abdelhady, M. A. Malik, P. O'Brien and F. Tuan, *J. Phys. Chem. C*, 2012, **116**, 2253; Q. Liu, A. Diaz, A. Prosvirin, Z. Luo and J. D. Batteas, *Nanoscale*, 2014, **6**, 8935.

16 C. Schliehe, B. H. Juareze, M. Pelletier, S. Jander, D. Greshnykh, M. Nagel, A. Merer, S. Foerster, A. Kornowski, C. Klinke and H. Weller, *Science*, 2010, **329**, 550; J. Li, Z. Chen, Y. Hu, X. Wang, T. Zhang, W. Chen and Q. Wang, *J. Am. Chem. Soc.*, 2013, **125**, 1213.

17 X. Zhang, W. Shi, J. Zhu, W. Zhao, J. Ma, S. Mhaisalkar, T. L. Maria, Y. Yang, H. Zhang, H. H. Hng and Q. Yan, *Nano Res.*, 2010, **3**, 643; H. Wan, J. Jiang, J. Yu, K. Xu, L. Miao, L. Zhang, H. Chen and Y. Ruan, *CrystEngComm*, 2013, **15**, 7649.

18 Y. Wang, Q. Zhu, L. Tao and X. Su, *J. Mater. Chem.*, 2011, **21**, 9248.

19 W. We, L. Mi, Y. Gao, Z. Zheng, W. Chen and X. Guan, *Chem. Mater.*, 2014, **26**, 3418.



 